Improved Understanding of Atomic Ordering in $Y_4Si_xAl_{2-x}O_{9-x}N_x$ Materials using a Combined Solid-State NMR and Computational Approach

V. R. Seymour[1,2]*, J. M. Griffin[1,2], B. E. Griffith[3], S. J. Page[3], D. Iuga[3], J. V. Hanna[3] and M. E. Smith[1,4,5]

1. Department of Chemistry, Lancaster University, Bailrigg, Lancaster, LA1 4YB, UK
2. Materials Science Institute, Lancaster University, Bailrigg, Lancaster, LA1 4YB, UK
3. Department of Physics, University of Warwick, Coventry, CV4 7AL, UK
4. Vice-Chancellor and President's Office, Building 37, University of Southampton, Southampton, SO17 1BJ, UK
5. Department of Chemistry, Building 59, University of Southampton, Southampton, SO17 1BJ, UK

Abstract

Ceramics based around silicon aluminium oxynitrides are of both fundamental structural chemistry and technological interest. Certain oxynitride crystal structures allow very significant compositional variation through extensive Si/N exchange for Al/O which implies a degree of atomic ordering. In this study, solid-state ^{29}Si MAS NMR and variable field 1D and 2D ^{27}Al MAS NMR measurements are combined with Density Functional Theory calculations of both the structural and NMR interaction parameters for various points across the $Y_4Si_2O_7N_2$-$Y_4Al_2O_9$ compositional range. This series provides numerous possibilities for significant variation of atomic ordering in the local ditetrahedral $(Si,Al)_2O_{7-x}N_x$ units. The two slightly structurally inequivalent aluminium sites in $Y_4Al_2O_9$ are unambiguously assigned to the observed resonances. Computational findings on $Y_4Si_2O_7N_2$ system demonstrate that the single observed ^{29}Si NMR resonance covers a range of local inequivalent silicon environments. For the first time, the MAS NMR and neutron diffraction data from the Y_4SiAlO_8N structure have been directly reconciled, thus establishing aspects of atomic order and disorder that characterise this system. This comparison suggests that, although the diffraction data indicates long range structural order supporting a highly crystalline character, the short range information afforded by the solid-state NMR measurements indicates significant atomic disorder throughout the $(Si,Al)_2O_{7-x}N_x$ units.

*Corresponding author
Valerie R. Seymour, Department of Chemistry, Lancaster University, Bailrigg, Lancaster, LA1 4YB, UK
Email: v.seymour@lancaster.ac.uk

1. Introduction

Silicon nitride-based ceramics are versatile materials, which have found numerous uses as refractories, cutting tools, microelectronics, engine wear parts and biomedical implants.[1,2] In forming components they are normally pressed into near shape as a powder and then sintered. However as very high sintering temperatures are required for pure Si_3N_4 often small amounts (a few wt%) of oxide are added (e.g., MgO, Al_2O_3, Y_2O_3, La_2O_3, or a combination thereof) to produce a liquid at significantly lower temperature thereby aiding sintering.[3-5] One of the most interesting systems is the addition of Y_2O_3 alone or in combination with Al_2O_3 as this system has been shown to form some of the most refractory phases in these systems.[4,5] The Y-Si-Al-O-N phase diagram[4] shows the formation of several stable crystalline phases, including an yttrium nitrogen-melilite ($Y_2Si_3O_3N_4$), and $Y_4Si_2O_7N_2$ (sometimes termed J-phase or N-YAM). Three crystalline phases exist in the Y_2O_3-Al_2O_3 system – yttrium aluminium garnet ($Y_3Al_5O_{12}$, YAG), yttrium aluminium perovskite ($YAlO_3$, YAP) and yttrium aluminium monoclinic ($Y_4Al_2O_9$, YAM).[6]

In silicon aluminium oxynitrides (sialons) and closely related materials, aluminium substitutes for silicon while oxygen concomitantly substitutes for nitrogen. This can create some extensive solid solution possibilities due to the closely matched Si-N and the Al-O bond lengths. However, this implies that full stochastic atomic mixing is unlikely and some type of ordering or clustering occurs to maximise the number of Si-N and Al-O bonds. In the Y-Si-Al-O-N system a complete isostructural solid solution exists ranging from $Y_4Si_2O_7N_2$ to $Y_4Al_2O_9$.[4] Although the crystal structure is largely known, the precise details of the atomic ordering, especially in the intermediate Y_4SiAlO_8N (Si/Al N-YAM) phase, remains unknown. The key issues that hinder a more complete understanding of this phase are associated with the difficulties in isolating viable single crystals and pure single-phase materials. In addition, it is well known that in principle both Si/Al and O/N disorder can occur. This disorder is difficult to probe by X-ray based techniques such as diffraction (XRD) and pair distribution functions (XPDF) as the close electronic similarity of these pairs of elements provide very little contrast between different possible ordering schemes. Although there has been interest in the structure of the crystalline phases of the Y-Si-Al-O-N system for more than 40 years, it has become very topical again recently as the high stability of these phases has combined with the realisation that they can act as host matrices for rare-earth ions such as Ce^{3+} and Sm^{3+}. Such systems find application in solid-state lighting based around phosphor-converted light emitting diode sources, with a significant amount of recent activity examining this particular application.[7-9] Very recent papers in this area has included the $Y_4Si_2O_7N_2$-$Y_4Al_2O_9$ solid solution[10,11] and the intermediate phaseSi/Al N-YAM .[12-14] In these papers the point has been explicitly made that oxygen/nitrogen (O/N) ordering within such materials leads to different local coordinations of the active centres strongly influencing the emission properties and therefore the ordering needs to be better characterised.

NMR is an excellent probe for distinguishing local environments, providing the complete distribution rather than an 'average' environment. When magic angle spinning (MAS) was initially applied to inorganic solids to distinguish local coordinations, ^{27}Al and ^{29}Si were key nuclei.[15,16] MAS NMR spectra from ^{27}Al are more complicated to interpret than ^{29}Si because of the additional presence of residual second-order quadrupolar effects.[16-20] However, these residual effects scale inversely with the applied magnetic field such that higher fields usually significantly benefit NMR observation of the central transition of ^{27}Al MAS NMR spectra.[16-20] Since the early NMR reports on $Y_4Si_xAl_{2-x}O_{9-x}N_x$ and related materials there have now been very significant advances in solid-state NMR instrumentation and

methodology.[21] Advances have included the availability of much higher applied magnetic fields ($\geq$ 20 T) and very fast MAS which have led to very significant improvements in the ^{27}Al NMR spectra that can be acquired. There is also the use of two-dimensional (2D) multiple-quantum (MQ) MAS NMR techniques.[16,21-23] With recent advances in density functional theory (DFT) approaches for computational chemistry, structural problems for oxynitrides can be re-examined by calculating both the structure (and its ordering) and also the resulting NMR interaction parameters, thereby much more strongly constraining the different ordering of (O/N) within the proposed structures.

Given the importance of Y_2O_3 as an additive for improved sintering of Si_3N_4 the crystalline phases of Y-Si-O-N system provided a range of local environments SiO_xN_{4-x} ($0 \leq x \leq 4$) being studied in detail by ^{29}Si MAS NMR.[24-26] The structural similarity of lanthanum La-Si-O-N phases meant that they were also reported on and for the N-YAM phase will be referred to below.[27,28] For ^{27}Al more detailed NMR studies exist for the Y_2O_3-Al_2O_3 system where locally aluminium is only coordinated by oxygen.[29,30] In these materials, some aluminium positions are characterised by large quadrupolar interactions which thus limits the effectiveness of mid-range external magnetic field strengths and MAS frequencies for the study of these systems. Furthermore, in the (Y/La)-Si-Al-O-N phases, although clear changes in the resonance positions were again apparent for $AlO_xN_{4-x,}$ components, the discrete aluminium signals could not be fully resolved or characterised. [29,31,32]The NMR methodology presented combining high applied magnetic fields with DFT calculations to probe Si/Al and O/N ordering in β´-sialons[33,34] is applied here to crystalline $Y_4Si_xAl_{2-x}O_{9-x}N_x$ phases.

2. Experimental Methods

2.1 Samples and Phase Identification

In this work two samples of YAM and two samples of Si/Al N-YAM were studied. The YAM samples were prepared by direct sintering of the terminal oxides (Y_2O_3, α-Al_2O_3) and by the wet chemical technique of thermal decomposition and sintering of the nitrates or sulphates.[29,35] For N-YAM direct sintering of the Y_2O_3, SiO_2 and Si_3N_4 powders compacted into pellets at >1550^{o}C for ~2 hours under an oxygen-free nitrogen atmosphere.[25,35] For the intermediate phase both a wet chemical (1550^{o}C, ~30 hours) and direct powder sintering approach (1800^{o}C ~3 hours) were used.[35] The samples were furnace cooled by simply turning the furnace off resulting in an initial cooling rate of ~100 ^{o}C/min. To confirm the phase identification, laboratory powder XRD of the samples was performed on a Rigaku SmartLab instrument, using a 9 kW Cu-source generator. Typically, 5° to 90° 2θ ranges were investigated over ~20 mins, with a step size of 0.01°. The XRD patterns are shown in Figures S1 and S2 of the Supporting Information (SI). These show that for both the target phases dominate, but with some minor components. For YAM these are Y_2O_3 and YAP (with the latter also picked up by ^{27}Al NMR) plus an unidentified phase, all < 5%. For Si/Al N-YAM AlN (also seen in ^{27}Al NMR data) and Y_2O_3 (a few percent) are present plus an unidentified phase (see discussion Sec. 3.4.1).

2.2 Solid-State NMR

^{27}Al MAS NMR data from the Si/Al N-YAM systems were acquired at 9.4, 11.7, 14.1 and 20.0 T using Bruker Avance III HD-400, Avance III-500, Avance II-600 and Avance III HD-850 spectrometers. The measurements at all these fields were acquired under ultra-fast MAS

conditions using Bruker 1.3 mm probes that enabled MAS frequencies of ~60 kHz. At each field a 'non-selective' (solution) pulse time of 9 μs was measured on 0.1 M $AlNO_3$ from which a 'selective' (solids) π/3 pulse time was implemented using short 1 μs excitation pulses and recycle delays of 5 s. All ^{27}Al chemical shifts are reported against the 0.1 M $AlNO_3$ IUPAC reference ((δ_{iso} 0.0 ppm) via a secondary solid $Al(acac)_3$ sample (δ_{iso} = 0 ppm, C_Q = 3.0 MHz, η_Q = 0.15), with the most negative singularity set at −0.87 ppm at 16.4 T).[36] Corresponding 2D ^{27}Al MQMAS data were acquired at 9.4 and 20.0 T using a 3Q Z-filtered experiment[16,23]; these measurements utilised a ~3 μs multiple quantum excitation pulse, a ~1 μs conversion pulse, soft 20 μs Z-filter pulses, a 20 μs interpulse Z-filter delay, a recycle delay of 3 s and MAS frequencies of 60 kHz.

Additional 1D ^{27}Al MAS and 2D 3QMAS NMR data from the YAM and 1D ^{27}Al MAS from the Si/Al N-YAM systems were acquired at 16.4 T using a Bruker Avance HD-700 spectrometer. These measurements were undertaken using a Bruker 2.5 mm MAS probe which enabled MAS frequencies of 25-30 kHz. These 1D ^{27}Al MAS NMR data were acquired using a short flip angle of 0.7 μs, with signal averaging for 512-960 transients, and a recycle delays of 3-5 s. The corresponding 2D ^{27}Al MQMAS data were recorded using a split-t_1 shifted-echo pulse sequence, with a SPAM pulse.[37,38] These measurements were recorded with signal averaging for 960 transients for each of 256 t_1 increments of 40 μs, and recycle delays of 1 s. Given the similarity of the ^{27}Al NMR interaction parameters characterising these sites, sufficient t_1 increments were required to avoid truncation and consequent line broadening that precludes accurate simulation and extraction of these values. The indirect dimension of these 2D MQMAS data were referenced according to reference 38. The ^{29}Si MAS NMR data from the Si/Al N-YAM system were acquired at 8.45 T using a Bruker 7 mm HX MAS probe which facilitated MAS rates of ~3.5 - 4.0 kHz. Short excitation pulses and a recycle delay of 60 s were used. The ^{29}Si chemical shifts spectra were calibrated against the primary TMS IUPAC standard (δ_{iso} 0.0 ppm).

2.3 DFT

To aid understanding of the experimental NMR spectra, NMR parameters were calculated for the three structures (YAM, N-YAM and Si/Al N-YAM), modelling distributions of O/N for the last two, as well as Al/Si for the latter. For DFT calculations the crystal structures and ditetrahedral units used are detailed in the SI (Secs S2, S3). Calculations of the energies of the different possible structures and their corresponding NMR parameters were carried out using the CASTEP code (8.0 Academic Release)[40-43] on Lancaster University's High End Computer cluster. A planewave energy cut-off of 50 Ry (~680 eV) was used, and integrals over the Brillouin zone were performed using a k-point spacing of 0.05 $Å^{-1}$. The convergence of total energy and calculated NMR parameters with respect to the energy cut-off and k-point spacing was checked using the crystal structure for YAM. Details of the isotropic chemical shift referencing are given in the SI, section S4. For ^{27}Al, ^{17}O, ^{29}Si and ^{15}N there is a high degree of correlation ($R^2 \approx 1$), comparable with that obtained in the literature.[44-46] For ^{89}Y our correlation is not quite as good; a higher degree of correlation has been achieved in the literature using a broader dataset, but is sufficient for accurate assignment.[47,48] Structural parameters, atomic coordinates and unit cell parameters were obtained from experimental crystal structures in the literature.[10,49,50] Prior to the calculation of NMR parameters, geometry optimisation of the models was performed by allowing the atomic coordinates to relax within either a fixed unit cell or the optimised position in a fully relaxed cell.

3. Results and Discussion

3.1. Structural Background

The diffraction work that is used as the starting point for this work is given in Table 1, which includes high resolution neutron powder diffraction, noting that single crystal work on large single crystals has not been possible. Central to the structure are the ditetrahedral units which for N-YAM are $Si_2O_5N_2$ and YAM Al_2O_7 – Q^1 units with a single bridging bond. The non-bridging bonds form part of coordination polyhedra around the yttrium. The unit cells are shown in Figure 1, with the yttrium-centred polyhedra linked together to form columns parallel to the a-axis. Four different yttrium environments exist coordinated by oxygen and

Name		YAM	N-YAM	Si/Al N-YAM
Chemical Formula		$Y_4Al_2O_9$	$Y_4Si_2O_7N_2$	Y_4SiAlO_8N
Number of distinct crystallographic T sites	2	Al	Si	Al, Si (1:1)
Coordination number of T site	4	AlO_4	$SiO_{4-y}N_y$	$AlO_{4-y}N_y$; $SiO_{4-y}N_y$
Number of distinct crystallographic Y sites	4	YO_x	$YO_{x-y}N_y$	$YO_{x-y}N_y$
Number of distinct crystallographic O/N sites	9	OAl_2		
ICSD number of crystal structure used		63650[43]	81860[44]	239827[10]

Table 1. Summary of local structural units and crystal structures used in this study.

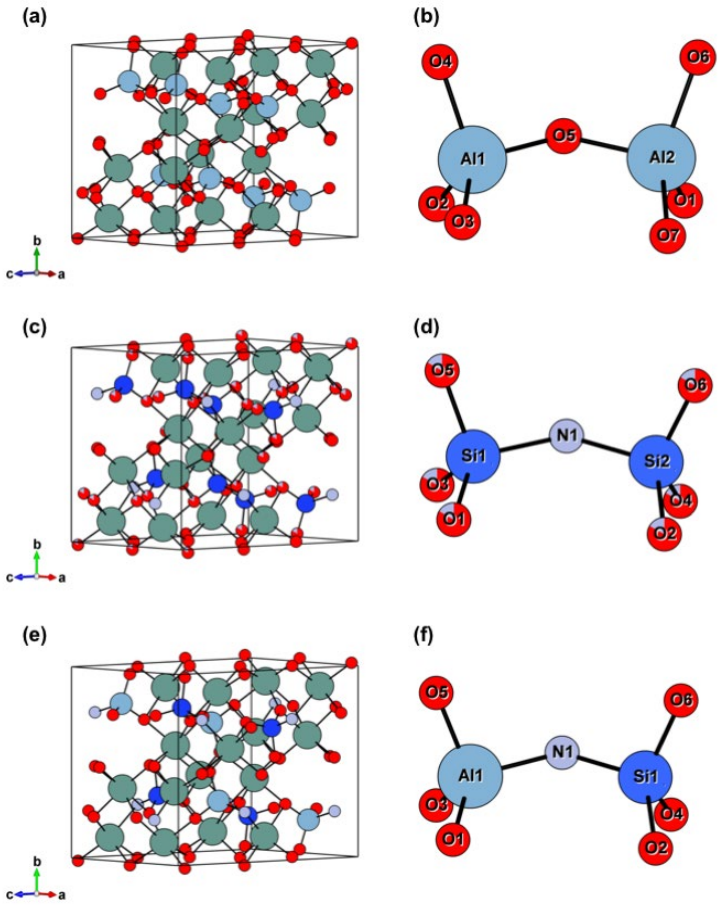

Figure 1: Unit cells and T site ditetrahedral pairs of the crystal structures of (a,b) YAM[43], (c,d) N-YAM[44], and (e,f) Si/Al N-YAM[10]. Distribution of Al/Si and O/N as defined in the CIF.

nitrogen atoms; three seven-coordinated and one six-coordinated. The nine oxygen and nitrogen atoms are distributed over the seven (one bridging, six non-bridging) sites of the Q^1 ditetrahedral unit and two 'ionic' sites connected to yttrium only. These sites provide much flexibility for oxygen/nitrogen disorder that can be difficult to unambiguously determine from diffraction alone. The additional complexity away from the end members is that there can also be silicon and aluminium disorder over the ditetrahedral units (i.e., Si-X-Si, Si-X-Al or Al-X-Al pairs, X=O, N; SI Sec. S3). Hence, there are some fundamental structural ordering questions that the methodology applied in this current study will provide new insight for.

In terms of crystal chemistry, site preferences are suggested by the concepts of Pauling in a series of 'crystal rules' which have been spelled out for oxynitrides by Morgan.[51] Pauling's Second Crystal Rule would indicate that for N-YAM the ionic sites (i.e., coordinated to yttrium only) should be occupied by oxygens to leave the ditetrahedral unit as $Si_2O_5N_2$. Within these units the bridging position should then be preferentially occupied by nitrogen. The disorder can further manifest itself as this 'average' ditetrahedral composition of $Si_2O_5N_2$ could be made up of a mixture of, for example, mostly likely Si_2O_6N, SiO_5N_2 and $Si_2O_4N_3$, although wider variations could also be present. The three most likely local compositions stated can all give a mixture of just SiO_2N_2 and SiO_3N local tetrahedra. For the yttrium system the crystal structure of N-YAM was refined using Rietveld refinement of X-ray data, but the similarity of the O/N scattering was unable to determine the O/N ordering. In the isostructural lanthanum N-YAM, neutron diffraction showed that all of the nitrogen was directly bonded to silicon, and with a ~90% occupancy of the bridging position[52], whereas for the lutetium variant (which is believed to be closer to the yttrium ordering) it is 100% in the bridging position.[53] A Monte Carlo (MC) analysis of the local configurations used the distributions determined for the lutetium and lanthanum N-YAMs, as well as an intermediate model of an equal distribution for the nitrogen not in the bridging position across the non-bridging positions.[48] The MC results suggest a deviation from the ordered 1:1 ratio of SiO_2N_2:SiO_3N, although the proportion of other units is low (typically ~5% for the most populated other coordinations).[54]

For the intermediate composition Si/Al N-YAM for the ditetrahedral unit there is a further compositional degree of freedom. In addition to O/N disorder there is also the potential for Si/Al disorder over the tetrahedral sites. As one progresses across the solid solution the slight polarisation across the ditetrahedral unit can occur depending on the degree of ordering, which can then subtly affect the nearby polarisation centres and their luminescent properties thereby pointing to the need for a better understanding the local ordering.[10,12] There have been two recent diffraction studies that have included Si/Al N-YAM. One based on XRD alone had the nitrogen solely occupying the bridging site leading to equal populations of SiO_3N and AlO_3N in an ordered structure.[12] The X-ray scattering lengths will have difficulty constraining the O/N distribution. More recently XRD and ND were combined, indicating the average probabilities were $SiO_{2.5}N_{0.5}$-$O_{0.5}N_{0.5}$-AlO_3.[10] This interestingly would contradict Pauling's Second Crystal Rule.

3.2. YAM, $Y_4Al_2O_9$

3.2.1 Experimental NMR Data

There have been previous solid-state ^{27}Al NMR studies of YAM. The earliest work, acquired at 8.45 T with a MAS rate of 3-5 kHz, was only able to observe a broad unnarrowed ^{27}Al lineshape relating to the YAM phase.[29] More recent work by Florian *et al.*[30] obtained good-quality ^{27}Al MAS NMR spectra at multiple fields (7.0-11.7 T) and faster spinning of up to

15 kHz, from which they were able to extract two components that contribute to the overall lineshape. However, there was strong overlap between the two ^{27}Al resonances and no 3QMAS NMR spectra were run.[30] ^{27}Al MAS NMR spectra obtained here are shown in Figure 2. These show a similar overall lineshape to that observed by Florian *et al.*, accounting for different field strengths. The additional sharper features are from well known impurities present in these samples. The broader feature of interest shows some discontinuities. Here two-dimensional (2D) MQ-MAS NMR spectra (16.4 and 20.0 T) are reported from YAM for the first time, which clearly separate the two sites (Figure 2). The lineshapes extracted from the 2D 3QMAS NMR spectrum at 16.4 T were fitted to obtain NMR parameters. These parameters were refined using the higher field (20.0 T) data by fitting[55] of 1D spectra [Table 2]. These values are in very good agreement with those obtained by Florian *et al.*, indicating that the previous study extracted these accurately despite the strong spectral overlap.

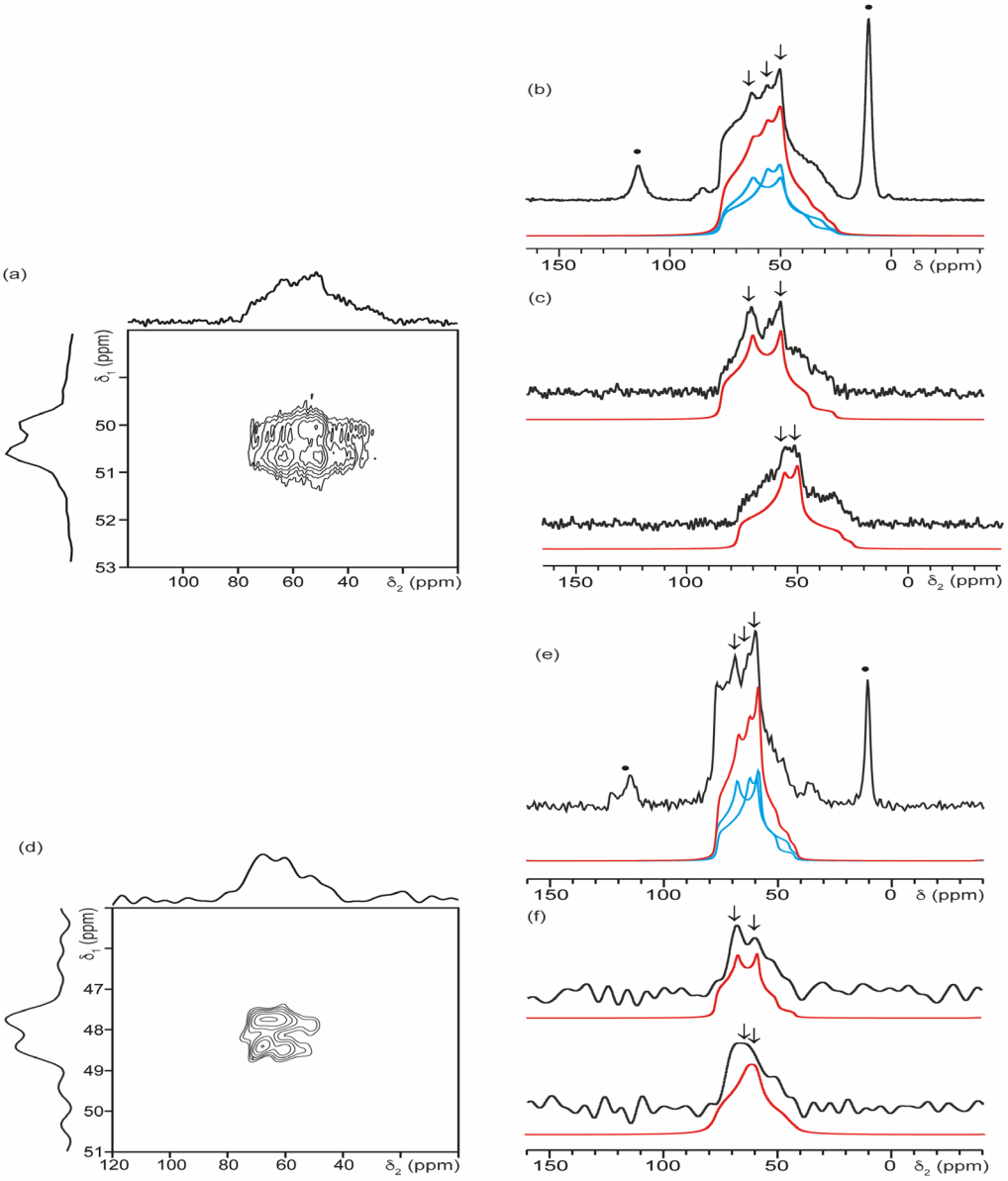

Figure 2: 1D ^{27}Al MAS NMR spectra and 2D ^{27}Al 3QMAS NMR spectra of YAM. (a,d) 2D ^{27}Al 3QMAS NMR spectra, (b,e) 1D ^{27}Al MAS NMR spectra, (c,f) extracted lineshapes from 2D spectra. (a-c) (25 kHz MAS, 16.4 T), (d-e) (25 kHz MAS, 20.0 T). Also shown are simulated spectra (red and blue) using the experimental NMR parameters given in Table 2. Key singularities are indicated (arrows) and impurities along with their sidebands (●).

3.2.2 Computational Methods and Site Assignment

The two crystallographically-distinct AlO_4 chemical environments in YAM show similar distortion, as discussed by Florian *et al.*[30] There are only small differences in the local oxygen coordination. The two ^{27}Al resonances therefore give very similar NMR interaction parameters which meant that to date there has been no assignment. Recently similar computational work using different functionals and optimisation has been reported, but no detailed structural assignment was reported.[56] Here CASTEP was used to aid spectral assignment, with the calculated ^{27}Al NMR parameters given in Table 2. There is good agreement with the previous calculated values.[56] These calculations enable the peaks in the experimental spectra to be assigned to the crystallographically-distinct sites. The similarity of the local geometry of the AlO_4 sites explains the closeness of the NMR interaction parameters. Experimentally the two sites have close isotropic chemical shifts differing by only 1.5-2 ppm. The quadrupolar interaction parameters (C_Q) are also close, differing by only ~4%. The C_Qs at ~10 MHz are large for AlO_4 sites in inorganic materials.[16,18-19] It is the difference in the asymmetry parameter (η_Q) that is most marked at 0.48 and 0.77 for the two sites, with extremely good agreement between the two experimental studies (here and, cf 30, Table 2). The CASTEP calculations for different cell optimisations are also given and shown in Table 2 and Figure 3. This data shows how important it is to optimise the structure as the parameters calculated from the unoptimised structure show much greater differences from the observed NMR parameters (Figure 3). In fully optimised relaxed cells (which is termed here relaxed cells) there is an offset in the absolute values of the shifts and C_Qs, with the calculated difference being ~1 ppm for the shifts and C_Qs differing by ~10%, but strong agreement in the trends and relative values. The computed η_Qs are 0.5 and 0.8, in very good agreement with the experimentally determined values. The corresponding relative shifts and C_Qs of the two sites are then all consistent (Figure 3). Hence the crystallographic site assignment is made in Table 2. As well as ^{27}Al NMR spectra, Florian *et al.* also obtained NMR spectra for ^{89}Y and ^{17}O (^{17}O-enriched sample),[30] adding to a previous report of the ^{89}Y MAS NMR data.[5] Here the ^{89}Y and ^{17}O NMR parameters are also computed, allowing site assignments, which are given in the SI (Sec. S5).

	^{27}Al NMR parameters			AlO_4 local environment			Al crystallographic site (CASTEP)/ assignment (Expt.)
	δ_{iso} (ppm)	C_Q/MHz [ν_Q/kHz]	η_Q	<Al-O> / Å (SD)	<O-Al-O> (°) (SD)	Ψ	
Expt.							
Florian *et al.*[30]	78.2 (±1)	10.8 [1622 (±30)]	0.48 (± 0.05)				1
	76.2 (±1)	10.4 [1554 (±30)]	0.77 (± 0.05)				2
This work	78.9 (±0.6)	10.7 (±0.1)	0.49 (±0.05)				1
	77.4 (±0.6)	10.3 (±0.1)	0.77 (±0.01)				2
Calc.							
CASTEP (Unoptimised)	83.50	7.95	0.72	1.72 (0.06)	109.37 (7.43)	0.66	1
	74.98	−8.37	0.57	1.80 (0.09)	108.97 (8.72)	0.80	2

CASTEP (fixed	78.06	10.33	0.48	1.75 (0.01)	109.04 (10.05)	0.94	1
cell)	77.00	9.97	0.82	1.76 (0.01)	108.87 (11.26)	1.13	2
CASTEP (fully	76.87	10.13	0.51	1.76 (0.01)	109.07 (10.22)	0.93	1
relaxed cell	75.97	9.83	0.81	1.77 (0.01)	108.90 (11.34)	1.15	2
PBEsol(1)[56]	76.8	10.71	0.49				
PBEsol(2)[56]	75.3	10.31	0.83				
LDA(1)[56]	76.3	11.25	0.50				
LDA(2)[56]	74.9	10.71	0.85				

Table 2. Experimental and calculated ^{27}Al NMR parameters for YAM: isotropic chemical shift (δ_{iso}), isotropic chemical shielding (σ_{iso}), quadrupolar coupling (C_Q), quadrupolar asymmetry parameter (η_Q). Also given are geometry parameters, average bond length (<Al-O>), average bond angle (<O-Al-O>), with standard deviation in brackets (SD), and the shear strain of AlO_4 polyhedron (Ψ).

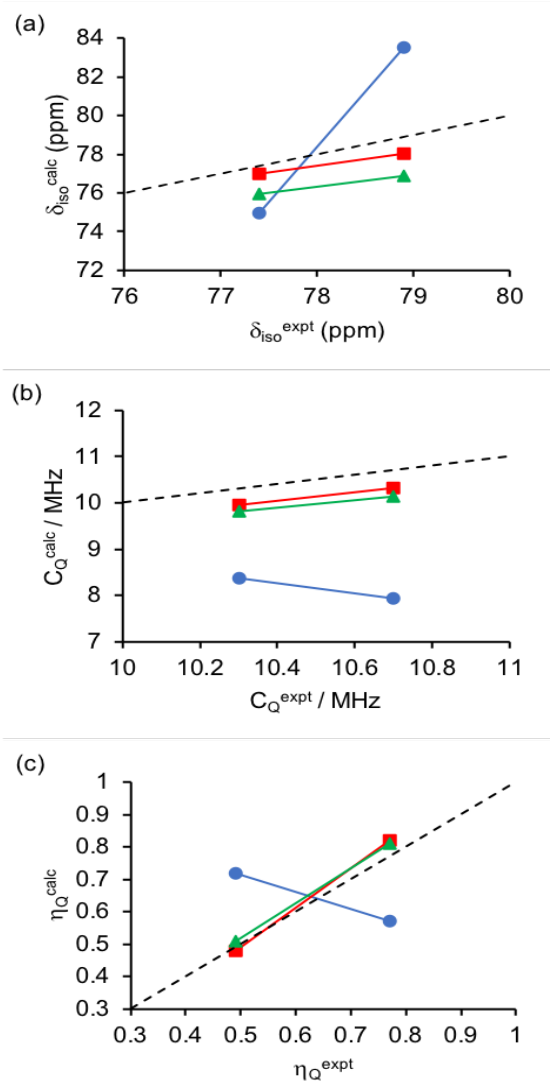

Figure 3. Comparison of experimental and calculated ^{27}Al NMR parameters for YAM, (a) isotropic chemical shift (δ_{iso}), (b) quadrupolar coupling (C_Q), and (c) quadrupolar asymmetry parameter (η_Q). Calculated values from structures as detailed in text which are: Blue circles (unoptimised structure), red squares (relaxed atomic positions within a fixed cell), and green triangles (fully relaxed cell and positions), with the dotted line showing where perfect agreement is.

3.3. N-YAM, $Y_4SiO_7N_2$

Literature values for the spin-½ nuclei in N-YAM (Table 3) provide a good basis for comparison with the calculations that are done here. Experimental ^{29}Si MAS NMR reveals what appears to be a single resonance with no structure.[25,26] This was taken to imply a single local silicon tetrahedral environment of SiO_3N based on the then current understanding of the ^{29}Si chemical shift sensitivities to local oxygen/nitrogen coordination which was expected to readily distinguish SiO_3N and SiO_2N_2.[24-26] The assignment to a single local coordination was also consistent with a brief report using neutron diffraction at the time.[57] However, subsequent ^{15}N MAS NMR data from a ^{15}N-enriched sample showed two resonances, well separated at 226.6 and 112.6 ppm, which can be assigned to the terminal NSi and bridging NSi_2 sites respectively.[58] This means that silicon must be in two distinct local environments (i.e., SiO_3N and SiO_2N_2). The implication is that shift difference between the SiO_3N and SiO_2N_2 in this phase is insufficient to provide spectral resolution. The NMR parameters calculated here for the different models are provided in the SI (Sec. S6), and summarised in Figure 4, allowing the origins of what is observed to be better understood. Looking at the data for N-YAM, the ranges the ^{29}Si chemical shift for Si1 and Si2 for different structural relaxations are shown for each of the possible local configurations, i.e. $SiO_2N_2^{b,t}$, SiO_3N^t and SiO_3N^b, where b and t indicate nitrogen occupies bridging and terminal positions respectively in the ditetrahedral unit. The experimentally determined range of δ_{iso} across the various studies is −73 - −74.4 ppm, with a corresponding linewidth covering 4 - 4.5 ppm.[25,26,59] Comparison of these ranges to the calculated values clearly shows that the ^{29}Si MAS NMR spectral resolution is indeed insufficient to distinguish which units are present, with the single experimental peak effectively covering all of the possible local configurations present. Although the calculations suggest that those models showing higher disorder across the ditetrahedral sites giving a population of $SiON_3$ up to ~7%[48] are probably not correct as one would expect an even broader ^{29}Si resonance.

In contrast, the calculated ^{15}N δ_{iso} show very distinct ranges for the different local environments (Figure 5). There is very good agreement between the ranges of the calculated values and the experimentally observed shifts. The experimental data shows that there are both bridging and terminal nitrogens with effectively equal populations. The calculations confirm the distribution suggested by the empirically-based Pauling Crystal Rules is quite closely followed. This is then also consistent with the experimental ^{29}Si MAS NMR spectrum being made up of two equally populated local coordinations, i.e. $SiO_2N_2^{b,t}$ and SiO_3N^b that are not resolved. As part of the computational work here the energies of the various structures are also determined which can be compared to the suggested atomic orderings from the Pauling Crystal Rules. Although the energy separation of the lowest energy structures for N-YAM is quite small (SI, Sec. S3) they do show that those containing nitrogen in the bridging position are favoured, agreeing with the Pauling Crystal Rules. It is also shown, again in accordance with the PCRs, that nitrogen occupying one of 'ionic' positions is strongly disfavoured. It is also clear that although the two silicon sites (Si1, Si2) are structurally inequivalent there is no strong preference for nitrogen to be associated with the terminal positions of one compared to the other. The structure calculations also back up the suggestion above that the O/N distribution tends to the more ordered end of the possibilities since local units that would occur in more disordered structures (e.g. SiN_4) are energetically unfavourable. This is further backed up by previous observations of the ^{17}O NMR interaction parameters and the calculations performed here. The ^{17}O MAS NMR spectrum from N-YAM shows several signals from the 'ionic' oxygen, i.e. bonded to yttrium only, and non-bridging

oxygens.[59,60] There is no clear evidence for any oxygen being in the bridging position of the ditetrahedral unit. It is worth comparing the yttrium N-YAM to the isostructural lanthanum variant. Two ^{29}Si MAS NMR studies showed a single resonance of comparable width, but shifted by ~10 ppm from the yttrium system.[27,28] The lanthanum system is supposed from the MC calculations to show more O/N disorder, with a significant fraction (~10%) of the bridging sites occupied by oxygen. However, the ^{17}O MAS NMR data from this system[59,60] shows a very good signal-to-noise ratio and no sign of any resonance from oxygen in the bridging position.

The calculated ^{89}Y isotropic chemical shifts, tabulated in the SI, for the lower energy models (1a-f, 3bi-ii) are consistent with the experimental data in Ref. 61, and whilst some of the other models deviate for experimental observations.

Reference (Ref.)	^{29}Si δ_{iso} (ppm) ±0.5	Local environment proposed in Ref.	^{89}Y δ_{iso} (ppm) ±7	Local environment proposed in Ref.	^{15}N δ_{iso} (ppm) ±2	Local environment proposed in Ref.
26	−73.7					
53	−73.6					
25	−74.4	SiO_3N				
52	−73	SiO_3N & SiO_2N_2			227 113	NSi t NSi_2 b
55			214	YO_x		

Table 3: Experimental ^{29}Si, ^{89}Y, and ^{15}N NMR parameters (isotropic chemical shift, δ_{iso}) obtained from the literature for yttrium N-YAM.

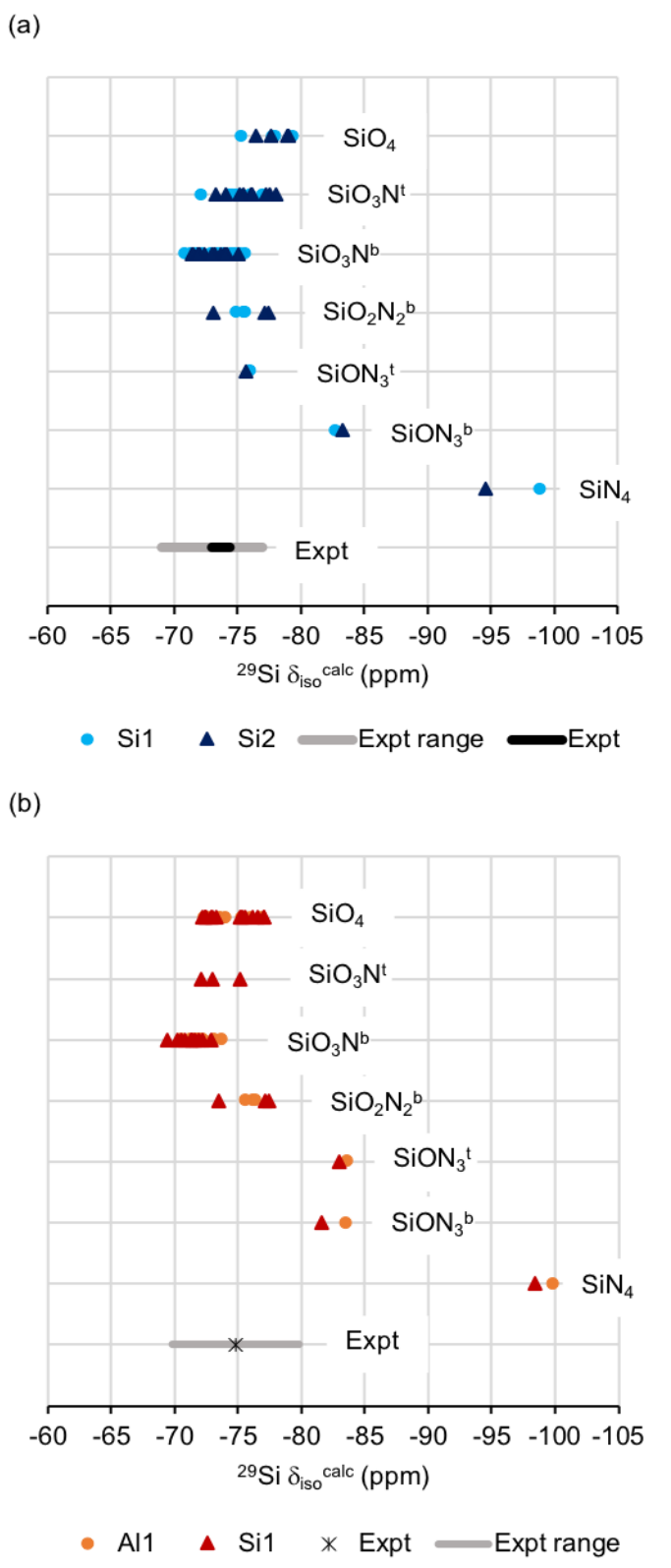

Figure 4: Plot of ^{29}Si isotropic chemical shift ranges calculated (CASTEP) for models of (a) (dark blue and light blue) N-YAM and (b) (red and orange) Si/Al N-YAM. The site labelling follows that of the published CIFs. In the CIF for Si/Al N-YAM the aluminium and silicon are on defined sites for fully ordered occupancy, Al1 and Si1 (Figure 1). In looking at the structural models created here the disorder placed some silicon onto the structural site designated as Al1 (i.e. see model ditetrahedral units in S3 of the SI). The original site label is retained for reference back to the original CIF ICSD 239827.

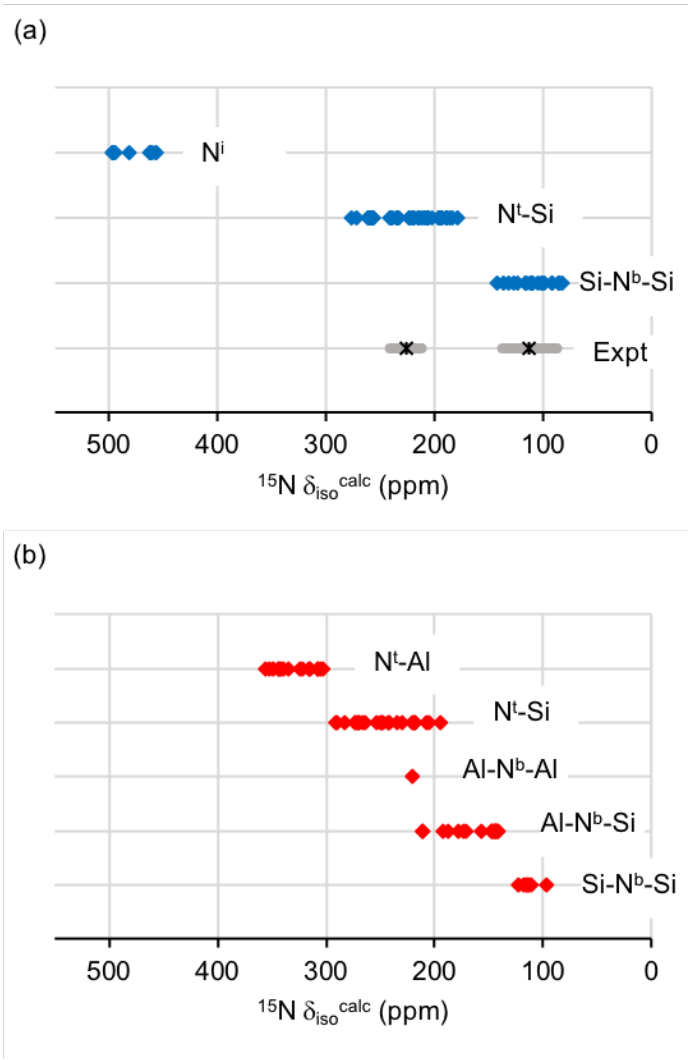

Figure 5: Plot of ^{15}N isotropic chemical shift ranges calculated (CASTEP) for models of (a) (blue) N-YAM and (b) (red) Si/Al N-YAM.

3.4. Si/Al N-YAM, Y_4SiAlO_8N

3.4.1 Experimental NMR Data

The different preparations of the intermediate Si/Al N-YAM here contained minor secondary phases. XRD shows small amounts of AlN in both the samples, which agrees with the ^{27}Al MAS NMR, with NMR also revealing small amounts of yttrium aluminate phases (see below) in the 1550 ^{o}C nitrate preparation. However, despite these secondary phases the main resonances associated with the Si/Al N-YAM can be identified, especially when combined with the computational work. ^{29}Si MAS NMR data [See SI, Sec. S7] shows that most of the silicon is in a single phase with a peak at −74.8±0.5 ppm and width of ~10 ppm, around twice that observed for the N-YAM end-member. This can be compared with −73.8 ppm and a linewidth of 4.2 ppm.[59] Hence there is only a small shift between the pure silicate N-YAM and the aluminium-containing intermediate version. It is again instructive to compare with the lanthanum variant. Previous ^{29}Si MAS NMR studies of the lanthanum N-YAM end member also showed a single resonance at −83.8 - −84.2 ppm with similar linewidths of ~ 3 ppm.[27,28] When aluminium is added to give $LaSiAlO_8N$, a peak in roughly the same shift position is obtained, but again significantly broader signal that was deconvolved into two equal intensity resonances at −80.8 and −85.6 ppm.[59] These were assigned to Si in $Si_2O_5N_2$ and $SiAlO_6N$

ditetrahedral units.[59] The ^{17}O MAS NMR spectrum from the aluminium-substituted sample shows three clear peaks, which is one more compared to the aluminium-free sample. The additional resonance at 311 ppm is assigned to non-bridging oxygens attached to aluminium, but again no bridging oxygen signal is observed.[54] In comparing the ^{17}O MAS NMR spectra in ref. 53 the lanthanum N-YAM sample appears to show no bridging oxygen signal, whereas in the aluminium-containing sample there may well be some broader underlying intensity.[59]

The other readily accessible nucleus for NMR in the Si/Al N-YAM system is ^{27}Al. The original NMR studies were hampered by the relatively modest magnetic fields of up to only 9.4 T then available. These early studies, as for $Y_4Al_2O_9$ showed narrow resonances from impurity phases and broad underlying, essentially unnarrowed intensity.[29,35,59] For the lanthanum analogue there was some sharper intermediate intensity peaking at ~57 ppm which is probably associated with AlO_4.[59] The ^{27}Al MAS NMR spectra obtained here at much higher, multiple magnetic field and MAS rates are shown in Figure 6.

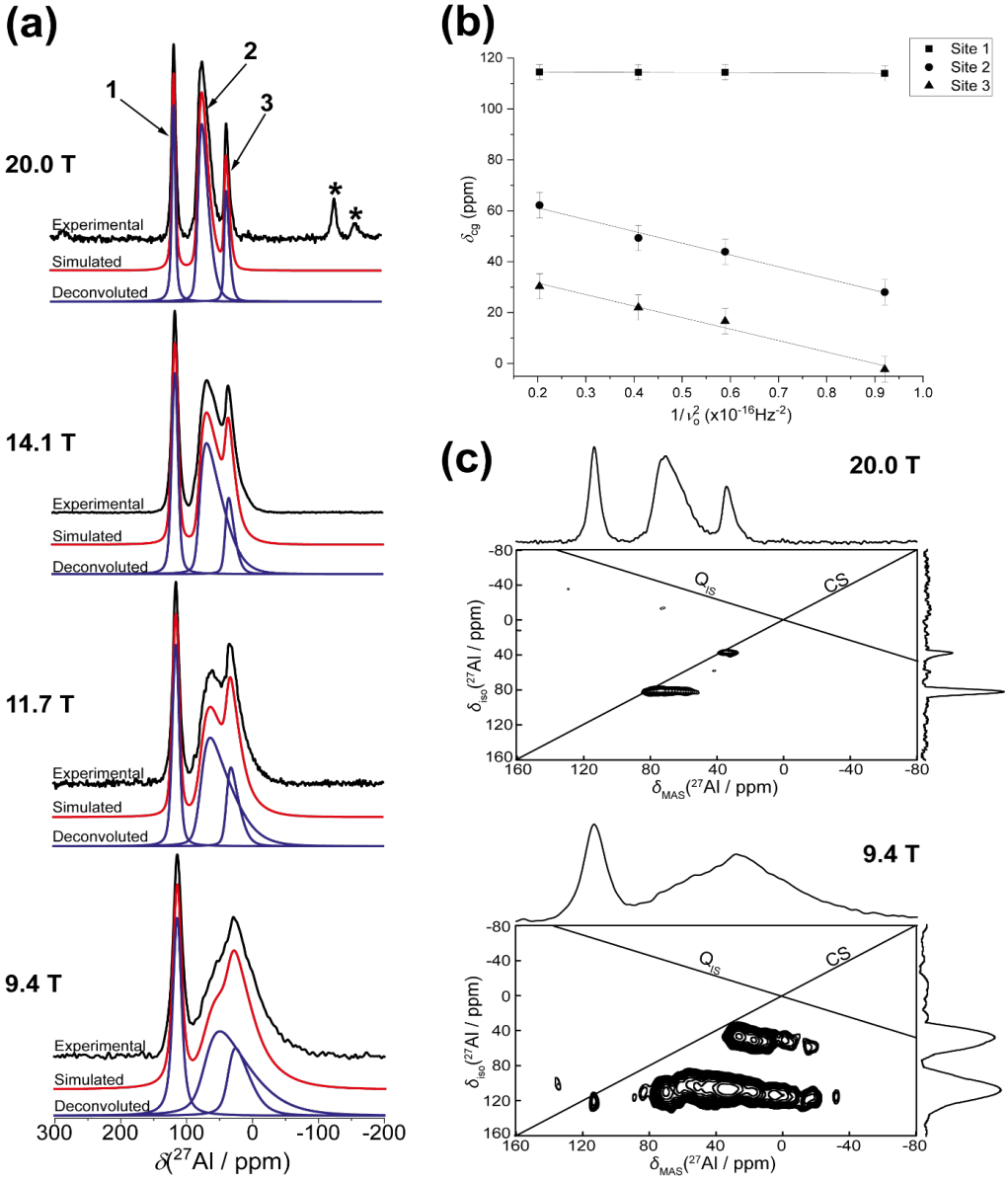

Figure 6 The (a) 1D ^{27}Al MAS NMR data (ν_r = 60 kHz) measured at 9.4, 11.7, 14.1 and 20.0 T, (b) graphical plots of the B_0 field variation of the centre-of-gravity shifts (δ_{cg}) from the 1D ^{27}Al MAS NMR data, and (c) 2D ^{27}Al MQMAS NMR data (ν_r = 60 kHz) from the Si/Al N-YAM (1800 °C) (where the direction of shifts caused by the isotropic chemical shift (CS) and second-order quadrupole shift (Q_{IS}) are indicated).

The multiple fields allow robust deconvolutions to be performed even with overlapping peaks (SI, Sec. S8). To ensure that the ^{27}Al NMR parameters were well constrained a comprehensive experimental methodology was applied. This included MAS at multiple magnetic fields (9.4 to 20.0 T) along with spectral simulation, the variation of the centre of gravity of the peak position with the magnetic field and simulation of the 3QMAS NMR data at two magnetic fields.[62,63] In addition, some subsets of the 1D ^{27}Al MAS NMR data were measured and simulated on multiple, independent occasions in order to reduce systematic errors in the analysis. There are a series of sharper impurity peaks, which the multiple applied magnetic fields show have only very small C_Qs (~0 MHz) (See SI Tables S7, S9 and S10). Both preparations show the major secondary phase at 114 ppm which is readily identified as AlN; also identified by XRD.[16,18] In the lower temperature synthesis there are two other very minor sharp peaks corresponding to only a few percent, with δ_{iso} at ~10.5 and 1.1 ppm which can be identified with the AlO_6 sites in $YAlO_3$ and $Y_3Al_5O_{12}$ respectively.[18,31] This then leaves a couple of broader peaks with intermediate shifts and significantly larger C_Qs between them. In the sintered sample there is a major peak (i.e., > 50% of the intensity, Table 4) with a δ_{iso} of ~81 ppm and C_Q of ~10.2 MHz. There is also a secondary peak with a δ_{iso} of ~40 ppm and C_Q of ~6.5 MHz. The lineshapes associated with the Si/Al N-YAM show a well-defined tail to lower shift (higher field) even at high external magnetic field strengths and MAS frequencies, suggesting that local structural disorder influences these phases. This disorder is characterised by a distribution of quadrupolar parameters rather than by significant levels of chemical shift dispersion, as exhibited by the specific directional contours in the 3QMAS NMR data of Figure 6(c). This phenomenon of high crystallinity and long-range order as determined by X-ray and neutron diffraction analyses being tensioned by short-range structural disorder and local variation as reported by solid state NMR analyses has been previously reported in studies of aluminoborate mullites.[64-66] From Table 4, the local disorder as captured in the C_Q width is quite pronounced being a significant fraction of the average C_Q.

Signal	QuadFit Simulation					Graphical fit		3QMAS Simulation	
	δ_{iso} (±2 ppm)	C_Q (±0.5 MHz)	C_Q Width (±0.5 MHz)	η_Q (±0.05)	Relative Intensity (±2 %)	δ_{iso} (±2 ppm)	P_Q (MHz)	δ_{iso} (±2 ppm)	P_Q (±0.5 MHz)
1	114	<1	<1	~0	26	115	1.1 ± 0.7	118	3.9
2	81	10.2	4.8	0.28	57	70	9.0 ± 2	81	8.8
3	39	6.5	3.1	0.06	17	41	9.0 ± 2	38	6.4

Table 4: A summary of the ^{27}Al NMR parameters derived from the data collected for Si/Al N-YAM (1800 °C). The δ_{iso}, C_Q, C_Q width, η_Q and relative intensity values reported from the QuadFit data are average values of the simulations undertaken of the 1D MAS NMR data measured and simulated at the B_0 fields (9.4, 11.7, 14.1, and 20.0 T) and then independently at 16.4 and 20.0 T. The δ_{iso} and P_Q values obtained from the 2D 3QMAS data are average values from the NMR ssNake simulations[63] of the data acquired at 9.4 and 20.0 T.

3.4.2 Computed NMR Interaction Parameters

NMR interaction parameters calculated using DFT approaches can greatly aid spectral understanding and examine if the atomic distribution (O/N and Si/Al) can be constrained. So both nitrogen/oxygen disorder around a ditetrahedral unit, and disorder (Si/Al) of the centres of the tetrahedra can occur. Neutron data suggested that the average composition of the

ditetrahedral unit is $SiO_{2.5}N_{0.5}$-$O_{0.5}N_{0.5}$-AlO_3, which could be realised through the oxygen and nitrogen distributing over the relevant sites of a unit $SiAlO_6N$. This could also be realised through first O/N disorder through the $SiAlO_5N_2$, $SiAlO_7$, with all ditetrahedral units strictly Si,Al pairs. However, if additional Al,Si disorder occurs this can then give e.g. Si_2O_6N, Al_2O_6N, $Si_2O_5N_5$, Al_2O_7, etc. The calculated ^{27}Al, ^{29}Si, and ^{15}N NMR parameters are given (SI Sec. S9) and are shown above for the spin-½ nuclei (summarised in Figs 4 and 5 above and shown more extensively in Sec. S10). The energies of the different structures show again several that are closely spaced, but those with the lower energies tend to again strongly support nitrogen in the bridging position (if attached to a silicon), and a preferred ordering where like-centred ditetrahedra form. This would then support that the ^{29}Si parameters, especially δ_{iso} would be expected to be very similar to the N-YAM end member. Then for the ^{27}Al NMR parameters the mixed coordination local tetrahedra i.e. AlO_3N tend to have smaller C_Q around 7-8 MHz (see SI Sec. S9, Table S11), whereas some of the AlO_4 in the energetically favourable structures have C_Q ~10 MHz. Such a value is in good agreement with the values extracted from the multiple magnetic field data simulations. The likelihood of this assignment is emphasised by examining the ^{27}Al MAS NMR spectra simulated for the calculated results using SIMPSON[67]for comparison with the experimental spectra (SI, Fig. S12). The simulations of the ^{27}Al MAS NMR lineshapes suggest that even though the Si/Al N-YAM phase is highly crystalline, there is a distribution of NMR interaction parameters. This is probably a result of some local disorder as a result of the distribution of the distinct ditetrahedral units throughout the structure. There is also the question of the interesting second major peak that spectral simulations suggest has a smaller C_Q of 6-7 MHz and a distinct shift of ~40 ppm. This is well outside of the range calculated for aluminium tetrahedra within the Si/Al N-YAM structure and also for such tetrahedra within β´-sialons.[34] However ref. 34 showed the shift could come from five-coordinated species. It is also interesting to compare to medium field data from lanthanum sialon glasses where a mixture of four-, five- and six-fold aluminium coordinations are present where a peak in this shift region occurs.[68] Two clear facts emerge: (i) the parameters of this peak are well determined from the comprehensive methodology applied here and show a very interesting δ_{iso}, and (ii) the combination of DFT shows categorically it does not reside on the Si/Al N-YAM structure. There is no obvious signature detected by XRD emphasising that solid-state NMR brings an important alternative perspective for characterising inorganic ceramic phases, especially when both atomic and structural disorder can occur with a mixture of phases. Although the structural origin of the peak is yet to be identified it looks like an intriguing local aluminium coordination in what is likely to be a disordered phase.

Conclusion

It has been shown that for YAM, ^{27}Al 3QMAS NMR spectra clearly separate the two aluminium resonances, supporting the work carried out previously by Florian *et al.*[30] The computational DFT (CASTEP) study presented here also enabled assignment of these two resonances to the two crystallographically-distinct sites. In the case of N-YAM the computational work here supported the experimental work of Hauck *et al.* For both N-YAM and Si/Al N-YAM, the computational studies show that for ^{29}Si, there are strongly overlapping δ_{iso} ranges for O/N mixed coordination local environments, and therefore a single experimental peak for ^{29}Si MAS NMR, cannot be used as *prima facie* evidence of a single silicon environment. The combination of experimental NMR data and computational work of the NMR interaction in an NMR crystallography approach allows much more insight into the structural detail, especially of Si/Al and O/N ordering. The computational studies also show

that ^{15}N is a useful indicator of local arrangements, however this information can only be accessed experimentally when samples have been ^{15}N enriched. In the N-YAM end member the computational work, considering ^{15}N, ^{17}O and ^{29}Si MAS NMR together, indicates that there is quite a good degree of O/N ordering, with the nitrogen taking the bridging site and then quite an ordered distribution over the other non-bridging sites. In the Si/Al N-YAM sample the NMR data suggests the local 'average' composition is not a good description and more disorder occurs over the different sites of the local ditetrahedral units. The ^{27}Al NMR parameters for the Si/Al N-YAM have been determined for the first time. The utility of applying an NMR crystallography approach which combines state-of-the-art experimental NMR data with computational work of both the structure and NMR interaction parameters is well illustrated here.

Supporting Information

Powder X-ray diffraction patterns, crystal structures and structural models used, chemical shift referencing for CASTEP calculations, CASTEP calculations of the ^{17}O and ^{89}Y NMR parameters for YAM, CASTEP calculations of the ^{29}Si, ^{15}N, ^{17}O and ^{89}Y NMR parameters for N-YAM, ^{29}Si MAS NMR spectrum of Si/Al N-YAM, ^{27}Al spectra, spectral simulations and NMR interaction parameters from Si/Al N-YAM at multiple magnetic fields, CASTEP calculations of the ^{27}Al, ^{29}Si, ^{15}N, ^{17}O and ^{89}Y NMR parameters for Si/Al N-YAM, Plots of DFT (CASTEP) calculated NMR Parameters for N-YAM and Si/Al N-YAM, and example SIMPSON input files.

Acknowledgments

Lancaster University is thanked for provision of the NMR, XRD and HEC facilities, and for funding this research. Characterisation facilities were part funded by the European Regional Development Fund (ERDF) under the collaborative Technology Access Program (cTAP). Dr Nathan Halcovitch (Lancaster University) is gratefully acknowledged for providing XRD support. The UK 850 MHz solid-state NMR Facility used in this research was funded by EPSRC and BBSRC (contract reference PR140003), as well as the University of Warwick including via part funding through Birmingham Science City Advanced Materials Projects 1 and 2 supported by Advantage West Midlands (AWM) and the European Regional Development Fund (ERDF). MES thanks the University of Southampton for its support of his research. JVH acknowledges financial support for the solid-state NMR instrumentation at Warwick which was funded by the EPSRC (grants EP/M028186/1 and EP/K024418/1) and the University of Warwick.

References

(1) Riley, F.L. Silicon nitride and related materials. *J. Am. Ceram. Soc.* **2000**, *83*, 245-265.
(2) Petzow, G.; Herrmann, M. Silicon nitride ceramics. *Structure and Bonding*, **2002**, *102*, 47-167.
(3) Jack, K.H. Sialons and related ceramics. *J. Mater. Sci.* **1976**, *11*, 1135-1158.

(4) Thompson, D.P. Phase relationships in the Y-Si-Al-O-N system. '*Tailoring Multiphase and Composite Ceramics'*, Eds Tressler, R.E.; Messing, G.L.; Pantano, C.G.; Newnham, R.E. **1986**, 79-91.
(5) MacKenzie K.J.D. Meinhold, R.H. Role of additives in the sintering of silicon nitrides: A ^{29}Si, ^{27}Al, ^{25}Mg and ^{89}Y MAS NMR and X-ray diffraction study. *J. Mater. Chem.* **1994**, *4*, 1595-1602.
(6) Cockayne B. The uses and enigmas of the Al_2O_3-Y_2O_3 phase system. *J. Less-Common Met.* **1985**, *114*, 199-206.
(7) Lu. F.C.; Song, X.P.; Liu, Q.L., Crystal structure and photoluminescence properties of $(Y_{1-x}Ce_x)_4Si_2O_7N_2$. *Opt. Mater.* **2010**, *33*, 91-98.
(8) Xia, Z.G.; Wu, W.W. Preparation and luminescence properties of Ce^{3+} and Ce^{3+}/Tb^{3+}-activated $Y_4Si_2O_7N_2$ phosphors. *Dalton Trans.* **2013**, *46*, 12989-12997.
(9) Wu, Q.; Yang, Z.; Zhao, Z.; Que, M.; Wang, X.; Wang, Y. Synthesis, crystal structure and luminescence properties of a $Y_4Si_2O_7N_2$:Ce^{3+} phosphor for near-UV white LEDs. *J. Mater. Chem. C* **2014**, *2*, 4967-4973.
(10) Wei, H.W.; Wang, X.M.; Kuang, X.J., Wang, C.H.; Jiao, H.; Jing, X.P. The structure, anion order, and Ce^{3+} luminescence of $Y_4Al_2O_9$-$Y_4Si_2O_7N_2$ solid solutions. *J. Mater. Chem. C* **2017**, *5*, 4654-4660.
(11) Hao, J.R.; Qu, X.Y.; Li, G.G.; Wang, H.Q.; Sun, Q.; Yan, C.J.; Al-Kheraif, A.A.; Lin, J. Solid-solution transformation and photoluminescence control in Ce^{3+}-doped $Ln_4Si_{2-x}M_xO_{7+x}N_{2-x}$ (Ln = Y, Lu; M = B, Al, P) oxonitridosilicate phosphors. *J. Alloys Compounds* **2019**, *776*, 224-235.
(12) Hua, Y.; Li, X.; Zhang, D.; Ma, H.P.; Deng, D.G.; Xu, S.Q. The crystal structure and luminescence properties of novel Ce^{3+} and Ce^{3+},Sm^{3+}-activated Y_4SiAlO_8N phosphors for near-UV white LEDS. *New J. Chem.* **2016**, *4*, 5458-5466.
(13) Hua, Y.; Zhang, D.; Ma, H.P.; Deng, D.G.; Xu, S.Q. Synthesis, luminescence properties and electronic structure of Tb^{3+}-doped $Y_{4-x}SiAlO_8N$:xTb^{3+} – a novel green phosphor with high thermal stability for white LEDs. *RSC Advances* **2016**, *6*, 113249-113259.
(14) Huo, J.S.; Dong, L.P.; Lu, W. Shao, B.Q.; You, H.P. Novel tunable green-red-emitting oxynitride phosphors co-activated with Ce^{3+}, Tb^{3+}, and Eu^{3+}: photoluminescence and energy transfer. *Phys. Chem. Chem. Phys.* **2017**, *19*, 17314-17323.
(15) Engelhardt G.; Michel, D. *High Resolution Solid State NMR of Silicates and Zeolites*. John Wiley & Sons, 1987.
(16) MacKenzie, K.J.D.; Smith, M.E. *Multinuclear Solid State NMR of Inorganic Materials*, Pergamon, 2002.
(17) Smith, M.E.; van Eck, E.R.H. Recent advances in experimental solid state NMR methodology for half-integer spin quadrupolar nuclei. *Prog. NMR Spectrosc.* **1999**, *34*, 159-201.
(18) Smith, M.E. Applications of ^{27}Al NMR techniques to structure determination in solids. *Appl. Magn. Reson.* **1993**, *4*, 1-64.
(19) Eden, M. ^{27}Al NMR studies of aluminosilicate glasses. *Ann. Rep. NMR Spectrosc.* **2015**, *86*, 237-331.
(20) Hauoas, M.; Taulelle, F.; Martineau, C. Recent advances in application of ^{27}Al NMR spectroscopy to materials science. *Prog. NMR Spectrosc.* **2016**, *94-95*, 11-36.
(21) Hanna, J.V.; Smith, M.E. Recent technique developments and applications of solid state NMR in characterising inorganic materials. *Solid State Nucl. Magn. Reson.* **2010**, *38*, 1-18.

(22) Medek, A.; Harwood, J.S.; Frydman, L. Multiple-quantum magic-angle spinning NMR: A new method for the study of quadrupolar nuclei in solids. *J. Am. Chem. Soc.* **1995**, *117*, 12779-12787.
(23) Brown, S.P.; Wimperis, S. Two-dimensional multiple-quantum MAS NMR of quadrupolar nuclei: A comparison of methods. *J. Magn. Reson.* **1997**, *128*, 42-61.
(24) Smith M.E. in *Solid-state NMR spectroscopy of inorganic materials*, Ed. Fitzgerald, J.J., *ACS Symposium Series* **1998**, *717*, 377-404.
(25) Dupree, R.; Lewis, M.H.; Smith, M.E. High-resolution ^{29}Si nuclear magnetic resonance in the Y-Si-O-N system. *J. Am. Chem. Soc.* **1988**, *110*, 1083-1087.
(26) Carduner, K.R.; Carter, R.O.; Rokosz, M.K.; Peters, C.; Crosbie, G.M.; Stiles, E.D. Silicon-29 magic-angle spinning nuclear magnetic resonance of sintered silicon nitride ceramics. *Chem. Mater.* **1989**, *1*, 302-307.
(27) Dupree, R.; Lewis, M.H.; Smith, M.E. A high-resolution NMR-study of the La-Si-Al-O-N system. *J. Am. Chem. Soc.* **1989**, *111*, 5125-5132.
(28) Harris, R.K.; Leach, M.J.; Thompson, D.P. Silicon-29 magic-angle spinning nuclear magnetic resonance of some lanthanum and yttrium silicon oxynitride phases. *Chem. Mater.* **1989**, *1*, 336-338.
(29) Dupree, R.; Lewis M.H.; Smith, M.E. Structural characterization of ceramic phases with high-resolution ^{27}Al NMR. *J. Appl. Cryst*. **1988**, *21*, 109-116.
(30) Florian, P.; Gervais, M.; Douy, A.; Massiot, D.; Coutures J.-P., A multi-nuclear multiple-field nuclear magnetic resonance study of the Y_2O_3-Al_2O_3 phase diagram. *J. Phys. Chem. B* **2001**, 105, 379-391.
(31) Butler, N.D.; Dupree R.; Lewis, M.H. The use of magic-angle spinning NMR in structural studies of Si-Al-O-N phases. *J. Mater. Sci. Lett.* **1984**, *3*, 469-470.
(32) Smith, M.E. Observation of mixed $Al(O,N)_4$ structural units by ^{27}Al magic angle spinning NMR. *J. Phys. Chem.* **1992**, *96*, 1444-1448.
(33) Cozzan, C.; Griffith, K.J.; Laurita, G.; Hu, J.G.; Grey, C.P.; Seshadri, R. Structural evolution and atom clustering in β-SiAlON: β-$Si_{6-z}Al_zO_zN_{8-z}$. *Inorg. Chem*. **2017**, *56*, 2153-2158.
(34) Seymour, V.R.; Smith M.E. Distinguishing between structural models of β´-sialons using a combined solid-state NMR, powder XRD and computational approach. *J. Phys. Chem. A* **2019**, *123*, 9729-9736.
(35) Smith, M.E. '*A high resolution multinuclear magnetic resonance study of ceramic phases*' PhD Thesis, University of Warwick, **1988**.
(36) Wong, G.; Smith, M.E.; Terskikh, V.V.; Wu, G. Obtaining accurate chemical shifts for all magnetic nuclei (^{1}H, ^{13}C, ^{17}O, and ^{27}Al) in tris(2,4-pentanedionato-O,O')aluminium(III) - A solid-state NMR case study. *Can. J. Chem.* **2011**, *89*, 1087-1094.
(37) Gan, Z.; Kwak, H.T. Enhancing MQMAS sensitivity using signals from multiple coherence transfer pathways. *J. Magn. Reson.* **2004**, *168*, 346-351.
(38) Ball, T.J.; Wimperis, S. Use of SPAM and FAM pulses in high-resolution MAS NMR spectroscopy of quadrupolar nuclei. *J. Magn. Reson.* **2007**, *187*, 343-351.
(39) Pike, K.J.; Malde, R.P.; Ashbrook, S.E.; McManus, J.; Wimperis, S. Multiple-quantum MAS NMR of quadrupolar nuclei. Do five-, seven- and nine-quantum experiments yield higher resolution than the three-quantum experiment? *Solid State Nucl. Magn. Reson.* **2000**, *16*, 203-215.
(40) Clark, S.J.; Segall, M.D.; Pickard, C.J.; Hasnip, P.J.; Probert, M.J.; Refson, K.; Payne, M.C. First principles methods using CASTEP. *Zeit. Kristall.* **2005**, *220*, 567-570.

(41) Pickard, C.J., Mauri, F., All-electron magnetic response with pseudopotentials: NMR chemical shifts. *Phys. Rev. B*, **2001**, *63*, 245101.
(42) Yates, J.R.; Pickard, C.J.; Mauri, F. Calculation of NMR chemical shifts for extended systems using ultrasoft pseudopotentials. *Phys. Rev. B* **2007**, *76*, 024401.
(43) Profeta, M.; Mauri, F.; Pickard, C.J. Accurate first principles prediction of ^{17}O NMR parameters in SiO_2: Assignment of the zeolite ferrierite spectrum. *J. Am. Chem. Soc.* **2003**, *125*, 541-548.
(44) Middlemiss, D.S.; Blanc, F.; Pickard C.J.; Grey, C.P. Solid-state NMR calculations for metal oxides and gallates: Shielding and quadrupolar parameters for perovskites and related phases. *J. Magn. Reson.* **2010**, *204*, 1-10.
(45) Mohamed, A.K.; Moutzouri, P.; Berruyer, P.; Walder, B.J.; Siramanont, J.; Harris, M.; Negroni, M.; Galmarini, S.C.; Parker, S.C.; Scrivener. K.L. *et al.* The Atomic-Level Structure of Cementitious Calcium Aluminate Silicate Hydrate. *J. Am. Chem. Soc.* **2020**, *142*, 11060−11071.
(46) Sun, H.; Dwaraknath, S.; Ling, H.; Qu, X.; Huck, P. ; Persso, K.A.; Hayes, S.E. Enabling materials informatics for ^{29}Si solid-state NMR of crystalline materials. *npj Computational Materials* **2020**, *6*, 530.
(47) Moran, R.F.; Fernandes, A.; Dawson, D.M.; Sneddon, S.; Gandy, A.S.; Reeves-McLaren, N.; Whittle, K.R.; Ashbrook, S.E. Phase Distribution, Composition, and Disorder in Y-2(Hf,Sn)(2)O-7 Ceramics: Insights from Solid-State NMR Spectroscopy and First-Principles Calculations., J. Phys. Chem. C **2020**, *124*, 17073−17084.
(48) Bashian, N.H.; Abdel-Latif, S.; Zuba, M.; Griffith, K.J.; Ganose, A.M.; Stiles, J.W.; Zhou, S.; Scanlon, D.O.; Piper, L.J.F.; Melot B.C. Transition Metal Migration Can Facilitate Ionic Diffusion in Defect Garnet-Based Intercalation Electrodes. *ACS Energy Lett.* **2020**, *5*, 1448−1455.
(49) Lehmann, M.S.; Christensen, A.N.; Fjellvag, H.; Feidenhans'l, R.; Nielsen, M., Structure determination by use of pattern decomposition and the Rietveld method on synchrotron X-Ray and neutron powder data; the structures of $Al_2Y_4O_9$ and I_2O_4. *J. Appl. Cryst*. **1987**, *20*, 123-129.
(50) MacKenzie, K.J.D.; Gainsford, G.J.; Ryan, M.J. Rietveld refinement of the crystal structures of the yttrium silicon oxynitrides $Y_2Si_3N_4O_3$ (N-Melilite) and $Y_4Si_2O_7N_2$ (J-phase). *J. Eur. Ceram. Soc.* **1996**, *16*, 553-560.
(51) Morgan, P.E.D. Pauling 2nd crystal rule for nitrogen-substituted crystal-structures. *J. Mater. Sci.* **1986**, *21*, 4305-4309.
(52) Takahashi, J.; Yamane, H.; Hirosaki, N.; Yamamoto, Y.; Suehiro, H.; Kamiyama, T. Shimada, M. Crystal structure of $La_4Si_2O_7N_2$ analyzed by the Rietveld method using time-of-flight neutron powder diffraction data. *Chem. Mater.* **2003**, *15*, 1099-1104.
(53) Takahashi, J.; Yamane, H.; Shimada, M.; Yamamoto, Y.; Hirosaki, N.; Mitomo, M.; Oikawa, K.; Torii, S.; Kamiyama, T. Crystal structure of $Lu_4Si_2O_7N_2$ analyzed by the Rietveld method using the time-of-flight neutron powder diffraction pattern, *J. Am. Ceram. Soc.* **2002**, *85*, 2072-2077.
(54) Takahashi, J.; Shimada, M.; Yamane, H. Local structures of $Si_2(O,N)_7$ ditetrahedra in J-phase. *Mater. Sci. Forum* **2007**, *554*, 43-49.
(55) Massiot, D.; Fayon F.; Capron, M.; King, I.; Le Calve, S.; Alonso, B.; Durand, J.O.; Bujoli, B.; Gan Z.H.; Hoatson G. Modelling one- and two-dimensional solid-state NMR spectra. *Magn. Reson. Chem.* **2002**, *40*, 70-76.

(56) Tu, B.T.; Liu, X.; Wang, H.; Wang, W.M.; Zhai, P.C.; Fu, Z.Y. Combining ^{27}Al solid-state NMR and first-principles simulations to explore crystal structures in disordered aluminum oxynitride. *Inorg. Chem.* **2016**, *55*, 12930-12937.
(57) Roult, G.; Bacher P. Liebaut, C.; Marchand. R.; Goursat P.; Laurent, Y. New tetrahedra in silicon oxynitride compounds. *Acta Crystallogr.* **1984**, *A40*, C226.
(58) Hauck, D.S.B.; Harris, R.K.; Apperley, D.C.; Thompson, D.P. Structural investigations of YAM-type yttrium silicon oxynitride by ^{15}N magic-angle spinning nuclear magnetic resonance. *J. Mater. Chem.* **1993**, *3*, 1005-1006.
(59) Leach, M.J. *Synthesis and multinuclear magnetic resonance studies of some nitrogen-containing ceramic phases*. PhD Thesis, University of Durham, **1990**.
(60) Harris, R.K.; Leach M.J.; Thompson, D.P. Nitrogen-15 and oxygen-17 NMR spectroscopy of silicates and nitrogen ceramics. *Chem. Mater*. **1992**, *2*, 260-267.
(61) Meinhold, R.H.; MacKenzie, K.J.D. Effect of lanthanides on the relaxation rates of ^{89}Y and ^{29}Si in yttrium silicon oxynitride phases. *Solid State Nucl. Magn. Reson.* **1995**, *5*, 151-161.
(62) Kemp, T.F.; Smith, M.E. QuadFit-A new cross-platform computer program for simulation of NMR line shapes from solids with distributions of interaction parameters. *Solid State Nucl. Magn. Reson.* **2009**, *35*, 243-252.
(63) van Meerten, S.G.J.; Franssen, W.M.J.; Kentgens, A.P.M. ssNake: A cross-platform open-source NMR data processing and fitting application. *J. Magn. Reson.* **2019**, *301*, 56-66.
(64) MacKenzie, K.J.D.; Smith, M.E.; Kemp, T.F.; Voll, D. Crystalline aluminium borates with mullite structure: A ^{11}B and ^{27}Al solid-state NMR study. *Appl. Magn. Reson.* **2007**, *32*, 647-662.
(65) Hoffmann, K.; Hooper, T.J.; Murshed, M.M.; Dolotko, O. Révay, Z.; Senyshyn, A.; Schneider, H.; Hanna, J.V.; Gesing, T.M.; Fischer, R.X. Formation, stability and Crystal Structure of Mullite-Type $Al_{6-x}B_xO_9$. *J. Solid State Chem.* **2016**, *243*, 124-135.
(66) Hoffmann, K.; Hooper, T.J.; Zhao, H.; Kolb, U.; Murshed, M.M.; Fischer, M.; Lührs, H.; Nénert G.; Kudějov, P.; Senyshyn, A.; Schneider, H.; Hanna, J.V.; Gesing, T.M.; Fischer, R.X. Crystal Chemical Characterization of Mullite-Type Aluminum Borate *Compounds J. Solid State Chem.* **2017**, *247*, 173-187.
(67) Bak, M.; Rasmussen, J.T.; Nielsen, N.C. SIMPSON: A General Simulation Program for Solid-State NMR Spectroscopy, *J. Magn. Reson.*, **2000**, *147*, 296-330.
(68) Leonova, E.; Hakeem, A.S; Jansson, K.; Stevensson, B.; Shen, Z.; Grins J.; Esmaeilzadeh, S.; Eden, M. Nitrogen-rich La–Si–Al–O–N oxynitride glass structures probed by solid state NMR. *J. Non-Cryst. Solids*, **2008**, *354*, 49-60.

TOC